Journal of The Electrochemical Society, **159** (5) B531-B540 (2012)
0013-4651/2012/159(5)/B531/10/$28.00 © The Electrochemical Society

Pt-Oxide Coverage-Dependent Oxygen Reduction Reaction (ORR) Kinetics

N. P. Subramanian,*,z T. A. Greszler, J. Zhang,* W. Gu,* and R. Makharia

General Motors Research and Development Center, Electrochemical Energy Research Lab, Honeoye Falls, New York 14472, USA

Oxygen Reduction Reaction (ORR) currents have been measured under the potential range of an operating fuel cell (0.72–0.9 Volts) while keeping proton and oxygen transport-related overpotentials insignificant by testing with pure O_2, at 100%RH and at low current densities. Low potential points are achieved by reducing the platinum loading on the cathode and operating under sub-ambient (<101.3 kPa_{abs}) pressure. The resulting experimental data are fit to Pt-oxide-coverage-dependent kinetics and the kinetic parameters extracted. The impact of Pt-oxide on apparent Tafel-slope transition (i.e., a function of potential) and on ORR performance is discussed.
 [DOI: 10.1149/2.088205jes]

Manuscript submitted December 24, 2011; revised manuscript received February 20, 2012. Published March 5, 2012. This was Paper 853 presented at the Boston, Massachusetts, Meeting of the Society, October 9–14, 2011.

Tremendous progress has been made in demonstrating required performance and durability of Polymer Electrolyte Membrane Fuel Cells (PEMFCs) for automotive application. The development focus is now shifting to cost reduction with a high emphasis on reducing the cathode platinum loading. Current demonstration levels typically are greater than 0.5 gm/kW which translates to >$3600 platinum/vehicle at today's Pt prices. Initial commercialization requirements are in the neighborhood of <0.1 gm/kW, whereas reaching <0.05 gm/kW would achieve the cost equivalent of the precious metal in modern catalytic convertor technology. The reaction rate for the hydrogen oxidation reaction (HOR)[1] on the anode is several orders of magnitude larger than that for the oxygen reduction reaction (ORR)[2] on the cathode. Hence very little Pt catalyst is needed to facilitate the anode reaction and the fuel cell kinetic losses are mainly controlled by the Pt loading used in the cathode. Over the years, there has been a significant amount of work focused on developing highly active ORR catalysts to reduce cathode Pt loading. Research effort on developing highly active cathode catalysts is incomplete, however, without a full mechanistic understanding of the ORR. In spite of decades of work, on oxygen reduction reaction using Pt and Pt alloys, there is still a disturbing lack of consensus on this mechanism.

ORR Rates are conventionally represented using simple Tafel kinetics:

$$i = i_0 \left(\frac{p_{o2}}{p_{o2,\text{ref}}} \right)^{\gamma} \exp\left(\frac{-\alpha F \eta}{RT} \right) \quad [1]$$

The Tafel slope (slope of the plot of cell potential vs. the logarithm of kinetic current density) is given by $\frac{2.303RT}{\alpha F}$ in units of volts/decade, where α is the transfer coefficient. Rotating disk electrode [RDE] experiments for ORR have shown a transition in Tafel slope from low values (a transfer coefficient of α∼1) at high potentials >0.85 V to high values (a transfer coefficient of α∼0.5) at low potentials <0.85 V.[3–5] In these RDE experiments, however, the observed currents at low potential (or high current density) are convoluted by the diffusion limited currents. The diffusion and kinetic processes are in series such that the kinetic currents can only be obtained by correcting the observed currents for the diffusion limited currents – a process which can introduce significant uncertainty. A cleaner approach is to measure kinetics without limitations from mass transport. Microelectrode studies, where the O_2 mass transport rates are significantly higher than in RDE, have also reported similar Tafel slope transitions.[6,7] Both RDE and micro-electrode experiments are, however, conducted ex-situ in liquid electrolyte which is substantially different from the fuel cell three-phase (gas-Nafion-catalyst) interface. Additionally, ORR measurements in liquid electrolyte are sensitive to contamination[8] and difficult to perform at temperatures (70–95°C) relevant to fuel cell operation. To date, there exists no direct measurement (in absence of significant mass-transport related overpotential) of ORR kinetic currents at both high and low potentials relevant to fuel cell operation.

Typically, ORR kinetics in PEMFCs are measured in pure O_2 at high potentials (∼0.85–0.9 V vs. RHE) and low current density. Most published literature report a Tafel slope of approximately 2.303 RT/F[2,9] (where α = 1). The true intrinsic exchange current density obtained by extrapolation to zero overpotential depends on the Tafel-slope value used for extrapolation. Variations in Tafel-slope used for extrapolation could result in large variation reported in the intrinsic exchange current density for ORR.[2] The kinetic currents at low potentials are obtained by extrapolation using the measurements at high potential and a Tafel slope of 2.303 RT/F. For fuel cell operation with conventional cathodes (0.4 mg_{-Pt}/cm^2, 50%Pt/V), the lowest potential range reached at realistic fuel cell conditions is still relatively high (high-frequency-resistance-corrected potentials >750 mV vs. RHE at 1.5 A/cm^2). Hence the constant Tafel-slope measured at high potentials has been sufficient to account for kinetic losses in such electrodes (after accounting for all known transport losses[10]). As the cathode loading is reduced, the potential range for fuel cell operation is shifted lower and performance with low precious metal loading (<0.1 mg Pt/cm^2) has been shown to diverge from 2.303 RT/F Tafel slope at high current densities, i.e. low voltage vs. RHE even after accounting for all known transport loss terms.[10,11] Several research groups have tried to understand the contribution of ORR kinetics and/or mechanism to this divergence in Tafel-slope.[12–15] One simple hypothesis for this divergence, presented by Uribe et al.[13] states that the ORR is poisoned by the presence of surface oxides such that the measured, apparent Tafel slope (2.303 RT/F) at high potential results from a combination of the intrinsic Tafel slope (2.303*2 RT/F) and the Pt-oxide surface coverage which is reduced as the potential decreases. Wang et al.[14,15] went one step further and explained the Tafel slope transition by a combination of relative activation barrier for the different reaction steps and the resulting Pt-oxide coverage. They used the double-trap reaction mechanism (O_2 -> OH*/O* -> H_2O) for their kinetic model and fit the experimental data for ORR and oxide coverage to extract the energies of the reaction steps and the individual OH and O coverage as a function of potential. From the model results, they concluded that at high potentials and above the reversible potential of O and OH transition, dissociative adsorption is fast (O_2 -> O*), the ORR is desorption limited and the resulting high O coverage inhibits ORR. At lower potentials, the O coverage drops, OH coverage increases, and the activation barrier for the reductive desorption (OH* -> H_2O) drops. As the OH coverage reaches a constant value, the Tafel slope is determined purely by the transfer coefficient, α. Another plausible explanation for the change in Tafel-slope is related to the efficiency of the electron transfer process. Oxygen can be reduced either by the

* Electrochemical Society Active Member.
z E-mail: nalini.subramanian@gm.com

direct four-electron transfer to give water or can proceed through the indirect successive two-electron transfer to form H_2O_2 and then H_2O or a combination of the direct and indirect pathway (parallel pathway). It is possible that not all the peroxide formed in the indirect pathway goes to water which results in a reduced kinetic current than predicted from the complete four electron transfer. According to Chen et al.[6], at conditions of high mass transfer rate, the H_2O_2 (formed in indirect pathway) may be convected away from the Pt, reducing the complete four-electron conversion to water. Nevertheless, based on these liquid electrolyte experiments, the contribution from the indirect pathway is negligible except at very low potentials close to the hydrogen adsorption region (<0.4 V) and may not explain the Tafel slope transition seen as high as ∼0.8 V.

The simple hypothesis for the effect of oxide coverage is drawn from a typical H_2/N_2 (anode/cathode) Cyclic Voltammogram (CV) as in an example shown in Figure 1a. The CV shown is measured on 50%Pt/Vulcan cathode using 200(1000)/50 SCCM 20%H_2 (in N_2)/N_2 in the anode and cathode respectively at 80°C, 100% relative humidity (RH). The Pt-oxide coverage is determined by dividing the charge under the Pt-oxide region, Q_O (>0.5 V) by the charge under the H^+ adsorption region, Q_H assuming one electron transfer per Pt atom.[16] In the example in Figure 1a, the Pt-oxide region in the cathodic direction is highlighted and is used to calculate Pt-oxide coverage during the cathodic scan. Alternatively, the Pt-oxide coverage in the anodic direction can also be calculated. Assuming negligible currents from HOR and/or other reactions (reactions from contaminants, for example) the total charge in the anodic direction should match the charge in the cathodic region. The resulting Pt-oxide coverage during both the anodic and cathodic CV scans is shown in Figure 1b. There is hysteresis in the Pt-Oxide coverage in the anodic and cathodic scans, but the oxide coverage increases with potential irrespective of the direction of scan. This oxide coverage effect can be incorporated into the ORR kinetic expression via a Temkin isotherm approach[17] as recently presented by Suzuki et al.[18] The resulting coverage-dependent kinetic expression is given by Equation 2.[19]

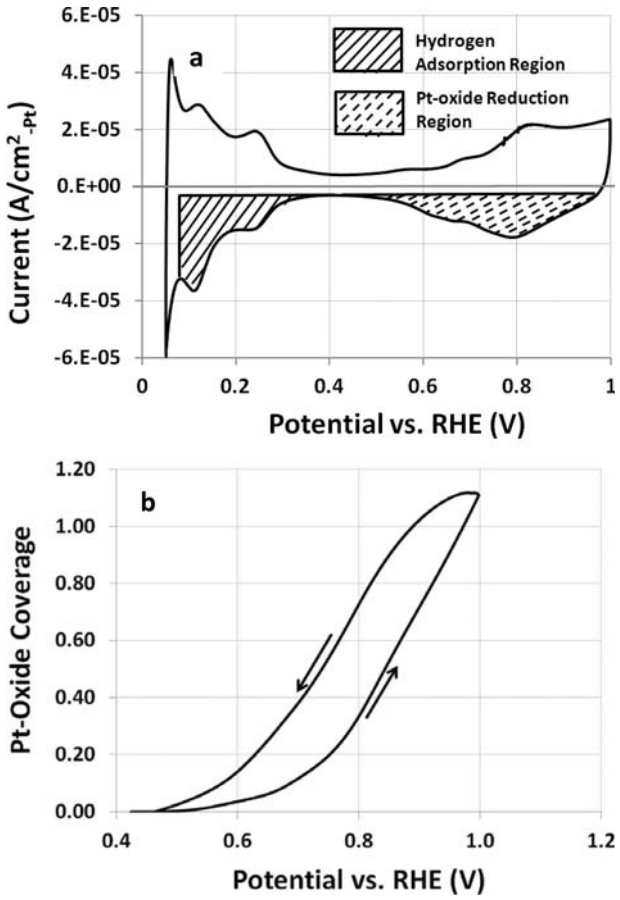

Figure 1. (a) Example Cyclic Voltammogram of 50%Pt/V cathode using 200(1000)/50 SCCM 20%H_2 (in N_2)/N_2 in the anode and cathode respectively at 80°C, 100%RH, (cathode Pt-loading is ∼0.4 mg_{-Pt}/cm^2_{-geo}, Pt surface area is ∼50 m^2_{-Pt}/g_{-Pt}, DuPont NRE211 membrane, proprietary diffusion media material discussed in experimental section). The two filled regions (solid and dashed lines) are integrated to obtain the total charge for Hydrogen Adsorption (Q_H) and Pt-Oxide (Q_O), respectively in the cathodic direction. (b) Pt-oxide coverage during the anodic and cathodic scans of the CV.

$$i = i_0 \left(\frac{p_{o2}}{p_{o2,\mathrm{ref}}}\right)^{\gamma} (1-\theta) \exp\left(\frac{-\alpha F \eta}{RT}\right) \exp\left(-\frac{\omega\theta}{RT}\right) \qquad [2]$$

where θ is the oxide coverage which is function of potential, ω is the energy parameter for the Temkin isotherm, which defines the coverage-dependent rate of change of the apparent Gibb's energy of adsorption of adsorbing species. This is a modification of the Tafel kinetics to account for the available Pt-surface area (i.e., 1-θ) and also the increase in the barrier to binding the ORR intermediates to Pt as the surface gets oxidized (i.e, the exponential coverage-dependent term, $\exp(-\frac{\omega\theta}{RT})$). At low Pt-oxide coverage, both the pre-exponential and the exponential coverage-dependent term have very little effect on the reaction rate. As the coverage increases, both the coverage-dependent terms will decrease the reaction rate. The above kinetic expression was shown to fit the performance of a proton exchange membrane (PEM) fuel cell,[18] where the surface coverage is varying with potential and time.[16]

Due to the lack of clear mechanistic understanding of ORR, there is also no clarity about the oxygen reaction order (γ) that is used in the rate expression. Neyerlin et al.[2] explained in detail the distinction between kinetic vs. total (kinetic+thermodynamic) reaction order that facilitates interpretation of the experimental data at various partial pressures to determine pure kinetic reaction order. They reported a total reaction order of ∼0.79 V. A total oxygen reaction order of 1[20] has also been used for modeling ORR in PEM cathodes. Recently, Uchimura et al.[21] fit the experimental ORR data at varying oxygen partial pressures and potentials (lowest potential is ∼0.8 V). They claimed that the potential-dependent oxide coverage results in an oxygen reaction order that varies with potential and made no attempts to determine the intrinsic ORR parameters. Estimation of true intrinsic ORR parameters is critical to gain insights into ORR mechanism. In our work here, the expressions for Tafel-slope and reaction orders are derived for coverage-dependent kinetic model and compared to those derived for the simple Tafel kinetic model.[2] It will be clear from this analysis that the apparent or the measured Tafel-slope and reaction orders at different potentials can be a combination of intrinsic and coverage-dependent terms.

Previous work[18,21] is complicated by the large uncertainty associated with proton and oxygen transport at high current density (and low potential) where the Tafel slope is expected to transition from the apparent to the intrinsic value. In our current work, experiments were conducted with operating conditions where the transport losses are minimal. H^+ transport through the membrane and electrode, and oxygen transport through diffusion media and electrode is facilitated by operating at 100%RH and pure O_2, respectively. Low cell potential is obtained without operating at high current density; this is achieved by reducing both the cathode platinum loading and the oxygen partial pressure. (i.e., operating in pure O_2 in vacuum).

Experimental

ORR polarization measurement.— Materials.— 50%Pt catalyst supported on Vulcan XC-72 carbon black was received from Tanaka Kikinzoku Kogyo K. K. (TKK), Japan and used as the cathode catalyst. The anode catalyst was 20 wt% Pt/Vulcan (TKK, Japan). Nafion D2020 (DuPont, USA) ionomer was utilized with an ionomer to carbon weight ratio of 0.95 and 0.6 in the cathode and anode,

respectively. The gas diffusion media used was proprietary. It has a carbon fiber paper backing (~200 μm) coated with a microporous layer (~30 μm). Nafion NRE211 (25 μm thick) was used as the membrane. 5 cm^2 catalyst-coated membranes (CCMs) prepared using the decal transfer method[22] were used for differential fuel cell performance tests, with a loading of ~0.40 or ~0.06 mg_{-Pt}/cm^2_{-geo} (geo-geometric) in the cathode and ~0.05 mg_{-Pt}/cm^2_{-geo} in the anode. The low loaded cathode (~0.06 mg_{-Pt}/cm^2_{-geo}) is diluted with Vulcan carbon to maintain the thickness of the electrode similar to that of the cathode loaded with ~0.4 mg_{-Pt}/cm^2_{-geo} (~12 μm) General procedure for electrode and MEA fabrication can be found in previously published literature.[22] We also tested the low-loaded cathode without diluting with carbon and hence a thinned electrode (results not shown in this paper), to see if there would be any effect on ORR due to extra carbon added with dilution. The results at low current density or the region used for ORR measurements were the same for the low-loaded parts with and without dilution. So, for the rest of the discussion we will focus on electrodes that were maintained at a constant thickness, i.e., ~12 μm.

Test procedure.—The conditions for measurement of O_2 polarization curves are 100% RH, 80°C, and high stoic of H_2/O_2 on anode/cathode at total pressures varying from ~252 kPa_{abs}(above-ambient) to ~62 kP_{abs}(below-ambient), corresponding to $p_{O2,channel}$ of ~204 to ~15 kPa. Sub-ambient operation was achieved through suction created using venturi operation. There is no pressure differential between the cathode and the anode, meaning that the H_2 partial pressure follows the O_2 partial pressure. As the H_2 partial pressure is varied, the onset potential for H_2 evolution also varies as governed by Nernstian relation.[23] This is taken into account to accurately reference the cathode potential vs. RHE universally (p_{H2}~101 kPa).

The O_2 polarization curves were measured by positive scan in HFR-free potential (HFR-High Frequency Resistance), with a hold time of 20 min.[2] at each potential (0.6,0.63, 0.65,0.7,0.725,0.75,0.775,0.8,0.825,0.85,0.875,0.9 V vs. RHE) as shown in Figure 2. The test stand operates in constant potential mode and dynamically controls to the HFR-corrected potentials using the feedback for HFR and current density. All potentials in this paper are stated vs. RHE unless specified otherwise. The current at each potential is determined by averaging the currents during the last one minute of the potential hold. Any kinetic treatment of the data is done only at <= 0.4 A/ cm^2_{geo} so that the effect of O_2 mass transport and electrode iR losses are negligible. Nevertheless, the potential trace is always maintained (0.6. . . . .0.9 V vs. RHE) irrespective of the cathode loading and O_2 partial pressure to consistently account for potential-dependent-oxide-coverage (detailed explanation of 'Oxide Coverage Measurement' is explained later in this 'Experimental' section). The error bars shown in the performance data represent the maximum and minimum range in current density for a sample size of three for each loading type.

Measurement of Pt-surface area.—Cathode Pt-surface area was measured by integrating hydrogen adsorption peaks as shown in Figure 1a (assuming 210 $\mu C/cm^2_{-Pt}$). The conditions of CV measurement were 30°C, H_2 in anode and with the cathode channels filled with liquid water. The liquid water that fills the cathode helps maintain hydrogen partial pressure by preventing any hydrogen (crossing over from anode) from diffusing out of the cathode. This prevents the H^+ adsorption peaks (required for Pt surface area analysis) from being masked by the hydrogen evolution current.[23] Pt surface area measured was ~45 and 35 m^2/g_{-Pt} for cathodes with 0.4 and 0.06 mg_{-Pt}/cm^2_{-geo}, respectively. The error in Pt-loading measurement may result in the differences observed in calculated Pt-surface area between the cathodes with different Pt-loadings. Nonetheless, the differences in ORR currents arising from loading differences are nullified by normalizing to Pt-surface area.

Measurement of high frequency resistance (HFR) and electrode proton transfer resistance.—The membrane and contact resistances and the electrode proton transfer resistances were measured as described by Liu et al.[24]. For the MEAs used in this work, HFR and cathode

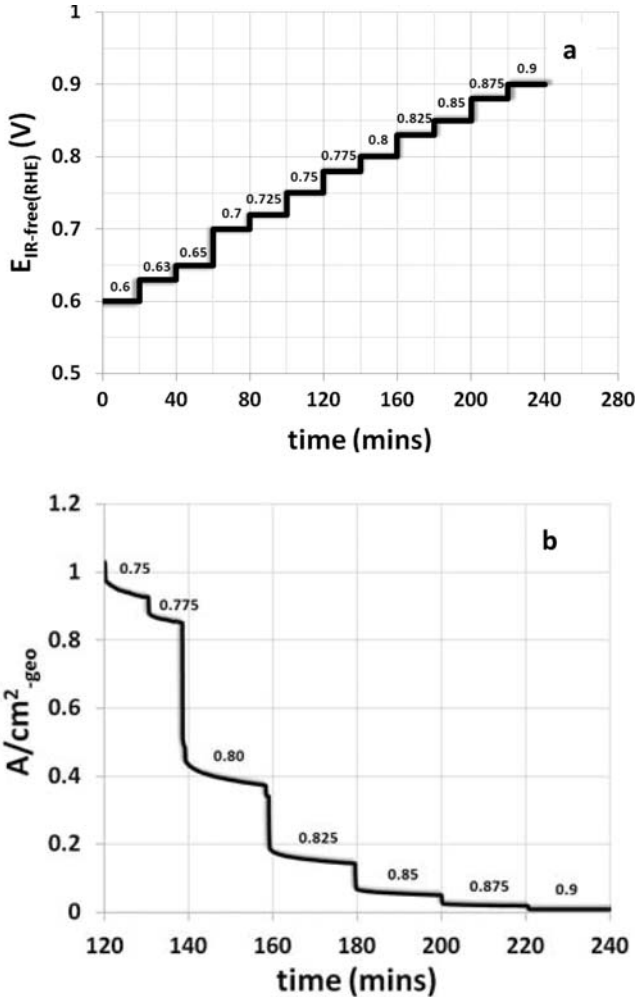

Figure 2. Examples for (a) Potential Profile for ORR measurement (b) Current profiles during the ~20 minutes hold at each potential. The current profile is only shown for a part but relevant portion (i.e. low geometric current density) of the potential range. Numbers in the label next to each step indicates cell potential, $E_{IR\text{-}free(RHE)}$ in V.

proton transfer resistance (12 μm thick cathode, irrespective of Pt loading) measured were ~0.05 and ~0.029 ohm-cm^2 respectively at the conditions used for polarization measurements (100%RH, 80°C). The losses from electrode proton transfer calculated as explained by Neyerlin et al.[25] for these conditions are less than 4 mV at low current densities (<= 0.4 A/cm^2_{-geo}); so non-polarizing membrane and contact resistances (HFR) dominate the iR corrections applied to the cell potential.

Oxide-coverage measurement.— Materials.— The materials for oxide-coverage measurements are the same as that for the ORR measurements with a few exceptions. A thicker membrane (50 μm thick, NRE212) was used to minimize H_2 crossing over from the anode to the cathode which interferes with Pt-oxide coverage measurements in the cathode. To maximize the signal to noise ratio of the potentiostat during Pt-oxide coverage measurements, 50 cm^2 CCMs were used. It was assumed, quite reasonably, in our opinion, that the oxide coverage is independent of cathode loading. Hence, measurements were carried out with a single cathode loading of ~0.4 mg_{-Pt}/cm^2_{-geo} while the anode was still maintained at ~0.05 mg_{-Pt}/cm^2_{-geo}.

Test procedure.—For this work, it is assumed that the oxide coverage on Pt is independent of oxygen partial pressure and gas environment

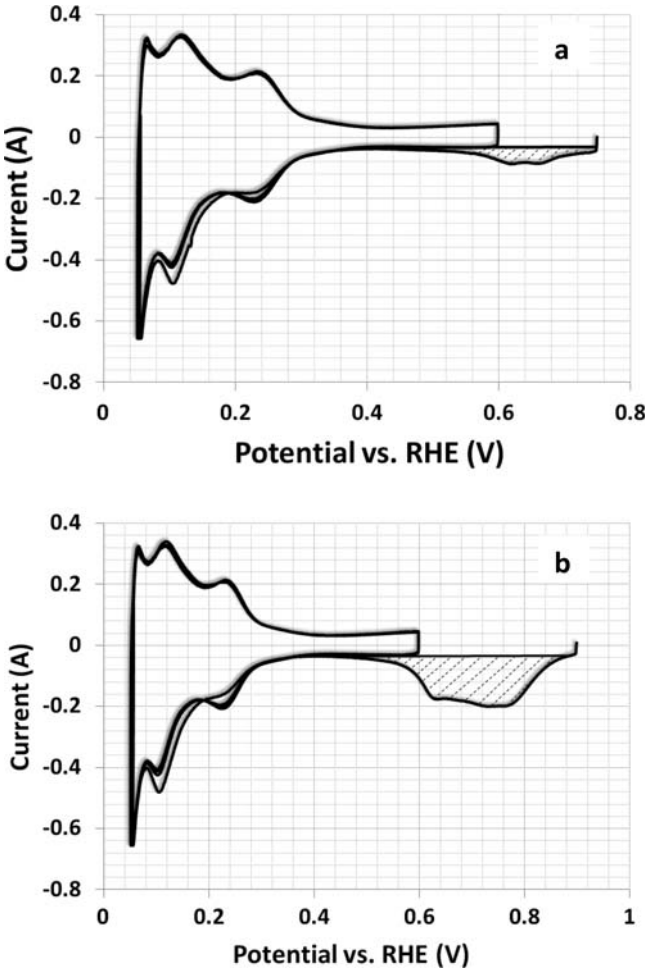

Figure 3. CV used for Pt-oxide measurement after 20 min. potential hold at each potential from 0.6 V (a) up to 0.75 V (b) up to 0.9 V. The filled regions are used to calculate oxide charge.

(N_2 or O_2).[26,27] The oxide measurements were carried out at 80°C, 101 kPa_{abs}, 100% RH, 200 sccm (1800 sccm) / 50 sccm of 10%H_2 (90%N_2) / N_2 on the anode / cathode. H_2-oxidation currents in the cathode (resulting from H_2 permeating from the anode) could vary as a function of potential. Any error in oxide coverage measurements induced by corrections for H_2 oxidation currents at different potentials is decreased by utilizing 10%H_2 in the anode and as mentioned earlier, a thicker, 50 μm membrane (NRE212).[27] The oxide kinetics is both potential and time dependent.[16] The oxide coverage on Pt at 0.6 V is measured after potential hold at 0.6 V for 20 min., oxide coverage at 0.63 V is measured after 20 min. hold each at potentials 0.6 and 0.63 V successively, and oxide coverage at 0.75 V is measured after 20 min. hold each at potentials 0.6, 0.63, 0.65, 0.7, 0.725, and 0.75 successively and so on. The calculated oxide charge via this method is referred to in this work as "cumulative oxide charge". This method of oxide coverage measurement ensures that the ORR current associated with the oxide coverage is measured using the same potential trace. The oxide that is built-up on the Pt surface during the potential hold is reduced by negative sweeps to 0.05 V vs. RHE at 20 mV/s scan rate. The resulting charge during the cathodic scan is used to calculate the oxide coverage.[27] Following the reduction by scanning to 0.05 V, two more CV scans are performed between 0.05 and 0.6 V to clean the surface before performing further oxide coverage measurements. Example CVs obtained after oxide buildup are shown in Figure 3. More details about the oxide coverage measurements can be found in the publication by Liu et al.[27]

Theory

The simple constant Tafel-slope kinetics has been considered by Neyerlin et al.[2] where they provided the definition of reaction order and Tafel-slope. These definitions are summarized in Table I.

The anode kinetic overpotential[1] and anode proton transfer losses are negligible under fully humidified conditions. Under operation where O_2 transport losses are negligible we can define the iR-free cell potential ($E_{IR-free}$) as given in Equation 3 below.

$$E_{IR-free} \simeq E_{cell} + i * HFR + i * R_{H^+}^{cathode} = E_{rev} - \eta \qquad [3]$$

where HFR and $R_{H^+}^{cathode}$ are the high frequency resistance (sum of membrane and contact resistances) and cathode proton transfer resistances, respectively. Both values have been measured experimentally and listed in the experimental section. E_{rev} is the reversible cell potential and η is the overpotential for ORR. E_{rev} and $E_{IR-free(RHE)}$ can be expressed as in Equations 4 and 5, respectively.

$$E_{rev} = E_{0(p_{H2},ref=p_{O2},ref=101\,kPa)} + \frac{RT}{4F} \ln\left[\left(\frac{p_{o2}}{p_{o2,ref}}\right)\left(\frac{p_{H2}}{p_{H2,ref}}\right)^2\right] \qquad [4]$$

$$E_{IR-free(RHE)} = E_{IR-free} - \frac{RT}{2F} \ln\left[\left(\frac{p_{H2}}{p_{H2},\,\mathrm{ref}}\right)\right] \qquad [5]$$

Equation 3 can be re-written as

$$\eta = E_{IR-free(RHE)} - E_{0(p_{H2},ref=p_{O2},ref=101\,kPa)} - \frac{RT}{4F} \ln \frac{p_{o2}}{p_{o2,ref}} \qquad [6]$$

where p_{H2} and p_{O2} are the partial pressures of H_2 and O_2 in the electrode, and $p_{H2,ref}$ and $p_{O2,ref}$ are the corresponding reference partial pressures (typically 101 kPa).

Table I. Reaction rate, reaction order and Tafel slope for simple Tafel vs. coverage-dependent ORR kinetic models.

Definition	Simple Tafel kinetics*	Coverage-dependent ORR model**
Reaction Rate***, J	$i_0\left(\frac{p_{O2}}{p_{O2,ref}}\right)^{\gamma} exp\left(\frac{-\alpha F\eta}{RT}\right)$	$i_0\left(\frac{p_{O2}}{p_{O2,ref}}\right)^{\gamma}(1-\theta)\,exp\left(\frac{-\alpha F\eta}{RT}\right) exp\left(\frac{-\omega\theta}{RT}\right)$
Kinetic O_2 Reaction Order, $\left(\frac{\partial logi}{\partial log p_{O2}}\right)_{\eta,T}$	γ	$\gamma - \left(\frac{x}{1-\theta} + \frac{\omega}{RT}\right)\left(\frac{\partial\theta}{\partial E_{IR-free(RHE)}}\right)\frac{RT}{4F}$
1/(Tafel slope), $\left(\frac{\partial logi}{\partial E_{IR-free(RHE)}}\right)_{p_{O_2},T}$	$-\frac{\alpha F}{2.303RT}$	$-\frac{\alpha F}{2.303RT} - \frac{1}{2.303}\left(\frac{1}{1-\theta} + \frac{\omega}{RT}\right)\left(\frac{\partial\theta}{\partial E_{IR-free(RHE)}}\right)$
Total O_2 Reaction Order (m), $\left(\frac{\partial logi}{\partial log p_{O2}}\right)_{E_{IR-free(RHE)},T}$	$\gamma + \frac{\alpha}{4}$	$\gamma + \frac{\alpha}{4}$

∗, ∗∗ α, ω and γ are assumed to be independent of $E_{IR\text{-}free(RHE)}$ and p_{O2}, $\theta = fn\left(E_{IR-free(RHE)}\right)$ and independent of p_{O2}.
∗∗∗ Overpotential used in the expression for reaction rate is defined as $\eta = E_{IR-free} - E_{rev}$ (or) $\eta = E_{IR-free(RHE)} - E_{o(p_{H2},ref=p_{O2},ref=1atm)} - \frac{RT}{4F}\ln\frac{p_{O2}}{p_{O2,ref}}$ where $p_{O2,ref}$ and $p_{H2,ref}$ are 101 kPa.

As discussed by Neyerlin et al.,[2] there are two definitions for reaction order - kinetic and total (kinetic+thermodynamic). The kinetic reaction order is defined at a constant overpotential while the total reaction order is defined at constant $E_{IR\text{-}free(RHE)}$ as given in Equation 7 and 8. Both reaction orders are defined at constant temperature.

$$\text{Kinetic Reaction Order} = \left(\frac{\partial \log i}{\partial \log p_{o2}}\right)_{\eta,T} \quad [7]$$

$$\text{Total Reaction Order} = \left(\frac{\partial \log i}{\partial \log p_{o2}}\right)_{EIR-free(RHE),T} \quad [8]$$

The definition of Tafel-slope is straightforward and is defined at constant oxygen partial pressure and temperature as given in Equation 9

$$\frac{1}{\text{Tafel} - \text{Slope}} = \left(\frac{\partial \log i}{\partial E_{IR-free(RHE)}}\right)_{p_{o2},T} \quad [9]$$

Using these definitions, the reaction order and Tafel-slope for the coverage dependent kinetics are derived here and compared to those of the simple Tafel kinetics[2] in Table I. The Tafel-slope for the coverage-dependent kinetics is not only dependent on α in the first term ($\frac{\alpha F}{2.303RT}$). The second coverage-dependent term ($\frac{1}{2.303}(\frac{1}{1-\theta} + \frac{\omega}{RT})(\frac{\partial\theta}{\partial E_{IR-free(RHE)}})$) modifies the Tafel-slope such that the experimentally observed or apparent Tafel-slope for the coverage-dependent kinetics is not a reflection of the intrinsic transfer coefficient, α, of the Tafel-kinetics. Similarly, the kinetic reaction order, γ, is modified by the coverage-dependent term $((\frac{1}{1-\theta} + \frac{\omega}{RT})(\frac{\partial\theta}{\partial E_{IR-free(RHE)}})\frac{RT}{4F})$ such that experimentally observed or apparent kinetic reaction order for the coverage-dependent kinetics is not a reflection of γ. It is evident from these definitions that for the coverage-dependent kinetics, the intrinsic parameters remain constant at all potentials. But, the apparent kinetic reaction order and the Tafel-slope have a coverage dependence and hence dependent on $E_{IR\text{-}free(RHE)}$, as explained previously by Gottesfeld and Uribe et al.[12,13] The total reaction order is defined at a constant $E_{IR\text{-}free(RHE)}$ and hence does not have any coverage dependence and is expressed as γ+α/4 for both the simple Tafel and coverage-dependent kinetics.

Results and Discussion

The results from O_2 polarization measurements are given in Figure 4 (a, b) for 0.4 and 0.06 $mg_{\text{-Pt}}/cm^2_{\text{-geo}}$, respectively, for varying $p_{O2,channel}$. Even though the potentials were scanned from 0.6 to 0.9 according to the profile shown in Figure 2a, only the data where the geometric current density was maintained at or below 0.4 $A/cm^2_{\text{-geo}}$ have been shown. The corrected potential is referenced to a reversible hydrogen electrode and is labeled $E_{IR\text{-}free(RHE)}$ after corrections for iR and O_2-transport losses, if any. Also shown in Figures 4a and 4b, using solid lines, are the model predictions assuming Tafel kinetics with a constant Tafel slope of 70 mV/dec. The parameters estimated by fitting the constant Tafel-slope model to each of the experimental data of ~0.4 and ~0.06 $mg_{\text{-Pt}}/cm^2_{\text{-geo}}$ cathode are labeled in Figures 4a and 4b. respectively and the average of the fit parameters are listed in Table II. The polarization curves at different $p_{O2,channel}$ for the electrode with the highest loading (Figure 4a) are all nearly parallel and follow the 70 mV/decade constant Tafel-slope kinetics. For the 0.06 $mg_{\text{-Pt}}/cm^2_{\text{-geo}}$ cathode, the polarization curves at different p_{O2} are not always parallel especially as the $p_{O2,channel}$ is decreased. The deviation from the 70 mV/decade kinetics is shown by the dashed line. The deviation seen experimentally here is as high as ~ 20 mV at the lowest potential explored in this work, i.e., at 720 mV. Neyerlin et al.[2] observed some points at low temperature (35°C) that deviate from constant Tafel-slope kinetics at $E_{IR\text{-}free}$ <800 mV, citing the presence of liquid water limiting oxygen diffusion at low temperatures. At higher temperatures, say 60°C, the lowest potential explored in their work was

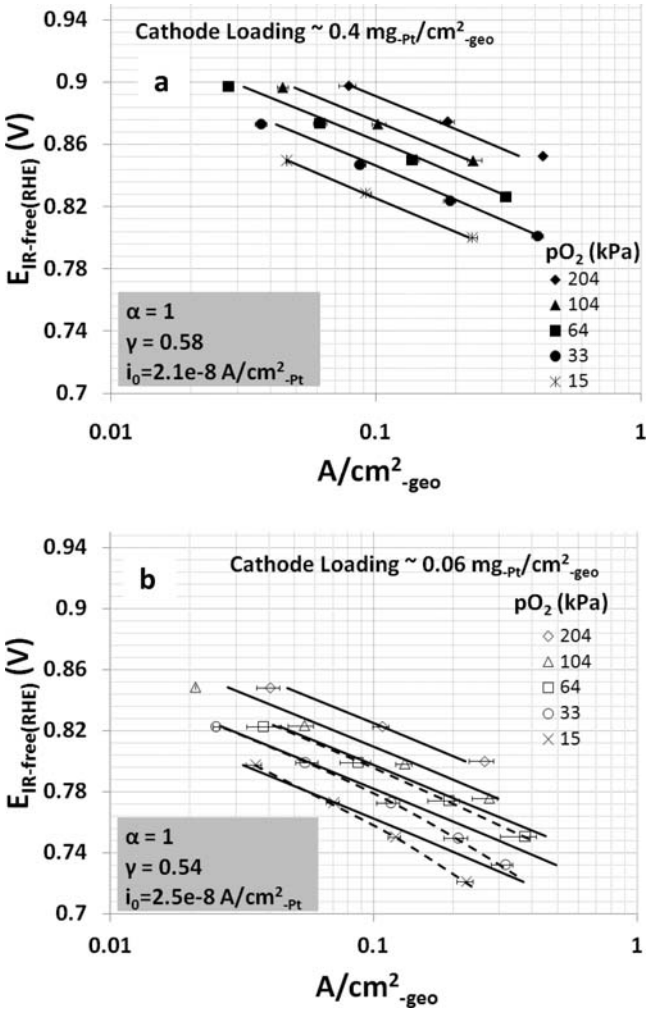

Figure 4. Experimental O_2 polarization curves at varying $p_{O2,channel}$ = 204/104/64/33/15 kPa for cathode loading of a) ~0.4 $mg_{\text{-Pt}}/cm^2_{\text{-geo}}$ and b) ~0.06 $mg_{\text{-Pt}}/cm^2_{\text{-geo}}$, symbols indicate experimental data, solid line indicates model predictions assuming constant Tafel-slope kinetics, dashed line indicates deviation of data from constant Tafel-slope kinetics.

~ > = 800 mV, and hence, not low enough to observe Tafel-slope transition, if any.

At this point, it is important to consider if the deviation of low-loaded electrode from the 70 mV/dec Tafel kinetics in Figure 4b can be attributed to transport-related losses that are not explicitly mentioned in Equation 3. As mentioned earlier, at 100% RH conditions and at geometric current densities <= 0.4 A/cm^2, the electrode proton transfer losses are lesser than 4 mV. Under pure O_2 and fully saturated conditions, there are no diffusive O_2 losses. The temperature rise in the electrode as the reaction proceeds depends on the thermal properties of the diffusion media (DM). As the saturation pressure of water vapor increases with increasing temperature, the $p_{O2,electrode}$ can be different from $p_{O2,channel}$. For the proprietary DM used in this study, the $p_{O2,electrode}$ normalized to $p_{O2,channel}$ and the corresponding potential losses in the electrode at different current densities are shown in Figures 5a and 5b respectively. The cell potentials are corrected for HFR, electrode iR losses (negligible) and any electrode p_{O2} losses. However, at current densities <= 0.4 $A/cm^2_{\text{-geo}}$, the electrode iR and p_{O2} losses are kept minimal such that the corrections due to these polarizing losses are no more than 5 mV. The total losses due to proton transport and p_{O2} drop in the electrode are shown in Figure 5c. Kinetic analysis is done at operating conditions where the total losses are <= 5mV as shown by the dashed line in the figure. Another source of voltage loss at relatively high current density (0.1–0.4 A/cm^2) and

Table II. Parameters estimated from the fit of Tafel kinetics vs. coverage-dependent ORR model.

Parameters	Simple Tafel kinetics		Coverage-dependent ORR model
	Ref. 2	This work	
α	1	1	0.5
γ	0.54 ± 0.02	0.56 ± 0.03	0.7 ± 0.08
m	0.79 ± 0.02	0.81 ± 0.03	0.83 ± 0.08
ω, J	NA	NA	3.0×10^3
i_0, A/cm^2-Pt	$2.47 \pm 0.3 \times 10^{-8}$	$2.3 \pm 0.3 \times 10^{-8}$	3.0×10^{-5}
$i_0^{(0.9\ V)}$, A/cm^2-Pt	$2.47 \pm 0.3 \times 10^{-4}$	$2.3 \pm 0.3 \times 10^{-4}$	1.6×10^{-4}

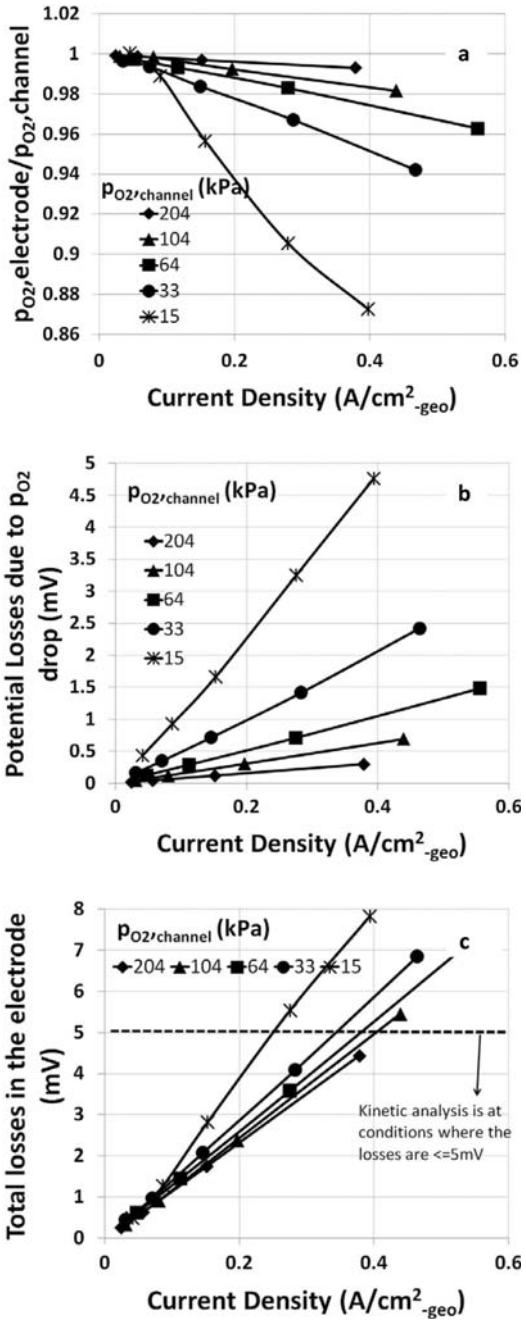

Figure 5. (a) Ratio of electrode to channel p_{O2} at different current densities (b) Potential loss due to drop in p_{O2} from channel to electrode (c) Total potential loss in the electrode due to p_{O2} drop and proton transfer.

low O_2 partial pressure can be attributed to oxygen transport through liquid water that may be present in the electrode. Experiments were performed under sub-saturated conditions (~90% channel RH) to ensure that the iR-free voltage response for the low-loaded electrodes is similar under 100%RH and slightly sub-saturated conditions (data not shown). Another possibility for the transition in Tafel slope could come from O_2 transport losses local to Pt.[11,28,29] The resistance for O_2 transport/dissolution through/into the ionomer film covering Pt-surface[28,29] is one possible origin for the local O_2 transport losses. The local transport resistances measured from limiting currents for the electrodes used in this work here is ~12 s/cm. (after correcting for bulk resistances). This resistance corresponds to a drop in p_{O2} of <2 kPa at 0.02 A/cm^2-Pt, the highest Pt-area normalized current density explored in this work. A 2 kPa drop results in only <= 3 mV losses and cannot account for ~20 mV losses seen with low-loaded electrodes at the lowest channel p_{O2} (~15 kPa) used in this work. These calculations and experiments confirm that the deviation of the low-loaded polarization curve from Tafel kinetics is indeed a kinetically limited phenomenon.

Average kinetic parameters extracted using Tafel kinetic assumptions for both 0.4 and 0.06 mg$_{-Pt}$/cm$^2_{-geo}$ loaded electrodes are listed in Table II. The intrinsic i_0 (defined at zero η), the exchange current density at 0.9 V at reference gas concentrations, i.e., $i_0^{(0.9\ V)}$, and the kinetic reaction order obtained in this study are similar to that obtained by Neyerlin et al. [2], also listed in Table II. Both studies used a transfer coefficient of $\alpha = 1$ in the Tafel kinetics. These results indicate that the data collected from two different studies are comparable.

The cumulative oxide coverage measured at each potential is shown in Figure 6a. As explained earlier, the oxide coverage on Pt is determined by assuming one electron transfer for every Pt atom. This is valid if the oxide species is assumed to be atop OH (Pt-OH) or bridge bonded O (Pt-O-Pt). But the assumption breaks down if oxide species is face-centered-cubic (fcc) or place-exchanged O.[30] XPS studies have shown increased oxide coverage in O_2 environment compared to N_2 environment.[31] Paik et al.[32] reported oxide coverage varying with p_{O2}. Another study by Liu et al.[26,27] concluded that there is no difference in the oxide coverage data between N_2 and O_2. Hence, it is not conclusive yet if the oxide coverage is a function of p_{O2}. In this study, the oxide coverage is assumed to be independent of p_{O2} and purely a function of Evs.RHE. Hence, oxide coverage determined from H_2/N_2 experiments as a function of potential vs. RHE is applied to data at all p_{O2}. As iR-corrections are negligible in a H_2/N_2 cell (no load), potential vs. RHE is also $E_{IR\text{-}free(RHE)}$. Figure 6b shows $\frac{d\theta}{dE_{IR-free(RHE)}}$ as a function of $E_{IR\text{-}free(RHE)}$ determined numerically from Figure 6a. The oxide coverage increases with potential. But $\frac{d\theta}{dE_{IR-free(RHE)}}$ increases up to about ~0.78–0.8 V and decreases above 0.8 V. This behavior indicates a Langmuir isotherm and Temkin isotherm type behavior for oxide growth <0.8 V and > 0.8 V, respectively. Above a critical coverage and hence potential, the energy of adsorption of adsorbing species decreases and the energy barrier for adsorption increases with increasing coverage indicating Temkin isotherm as observed by Sepa et al. for ORR.[17]

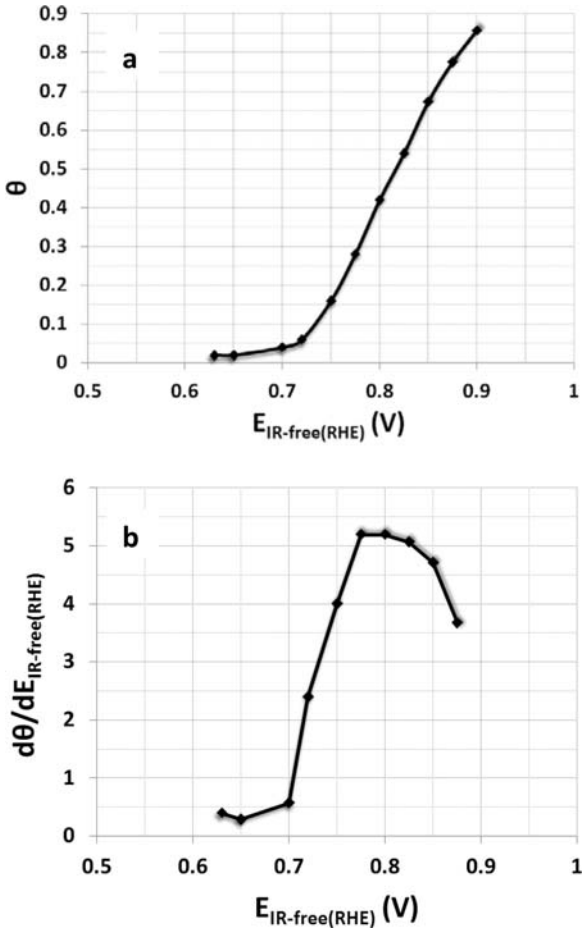

Figure 6. (a) Oxide coverage (b) $\frac{d\theta}{dE_{IR-free(RHE)}}$, both vs. $E_{IR\text{-}free(RHE)}$.

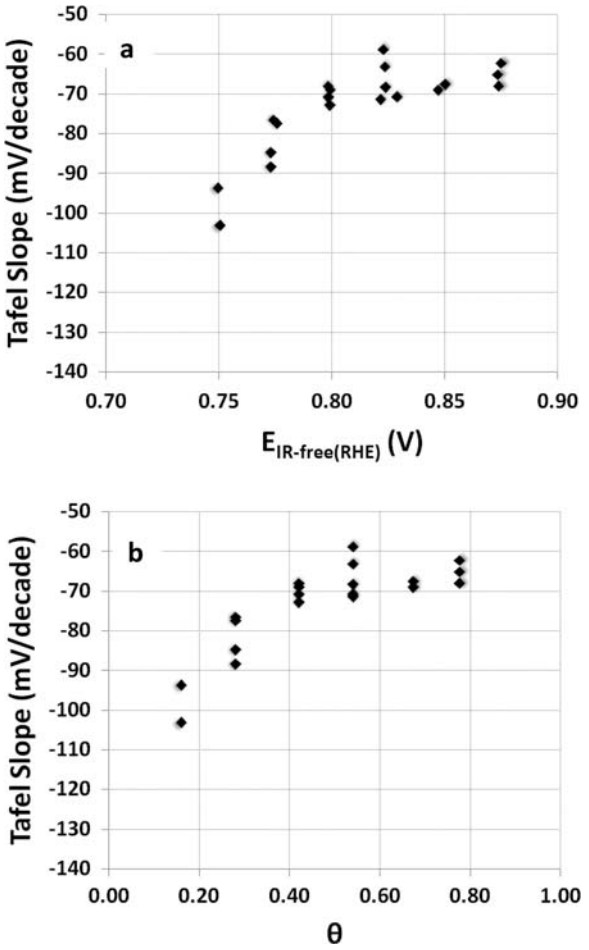

Figure 7. Tafel slope determined from the slope at each potential in Figure 4 a and b as a function of (a) $E_{IR\text{-}free(RHE)}$ and (b) Coverage.

The experimental Tafel-slope are determined from the slope of $E_{IR\text{-}free(RHE)}$ vs. log(i) at different potentials in Figure 4 and are plotted in Figure 7a. The slope at each potential is determined from the slope of the line connecting the adjacent experimental points on either direction of that potential (three-point slope). Since the oxide coverage (θ) at each potential is known (as shown in Figure 6a), the x-axis in Figure 7a is converted to θ and the resulting Tafel-slope as a function of θ is represented in Figure 7b. The Tafel slope is nearly constant, i.e., ∼ 70 mV/dec. at potentials >= 0.8 V vs. RHE (or θ of >= 0.4). At potentials <0.8 V vs. RHE (or θ <0.4), the Tafel slope increases and reaches ∼104 mV/dec. at ∼ 0.75 V vs. RHE (or θ ∼0.16). There could be some error involved in determining Tafel-slopes from experimental polarization curves, which could result in the spread, however minor, in the Tafel-slope at any $E_{IR\text{-}free(RHE)}$. There is also no obvious dependence of Tafel-slope on p_{O2} and the Tafel-slope can be assumed to be primarily a function of $E_{IR\text{-}free(RHE)}$.

To determine the parameters for the coverage-dependent ORR model, it is assumed that the intrinsic transfer coefficient is $\alpha = 0.5$ (i.e. Tafel-slope = 140 mV/dec. at 80°C). This leaves three unknown parameters; γ, ω and i_0. The equation for coverage-dependent-Tafel-slope listed in Table I is fit to the experimental Tafel-slope as a function of $E_{IR\text{-}free(RHE)}$. The input of θ and $d\theta/d(E_{IR\text{-}free(RHE)})$ to the Tafel-slope equation are determined numerically from Figures 6a and 6b. The fit of the model to the experimentally observed Tafel-slope is shown in Figure 8. The model fit was obtained by using $\omega = 3.0$ kJ. The model extrapolation to potentials lower than that explored experimentally indicates a Tafel-slope of 135 mV/dec. at 0.65 V vs. RHE and is expected to reach 140 mV/dec. at 0.6 V vs. RHE where the oxide coverage goes to zero. Figure 9 shows the plot of log i vs. log p_{O2} at different $E_{IR\text{-}free(RHE)}$. According to the definition of total reaction order in Table I, the slope of these plots at different $E_{IR\text{-}free(RHE)}$ should be the same (parallel lines) and should give the total reaction order ($m = \gamma+\alpha/4$). All the lines, each at different $E_{IR\text{-}free(RHE)}$, are nearly, but not strictly parallel, with an average slope of ∼0.83 and a standard deviation of 0.08. For the model fit of the experimentally apparent

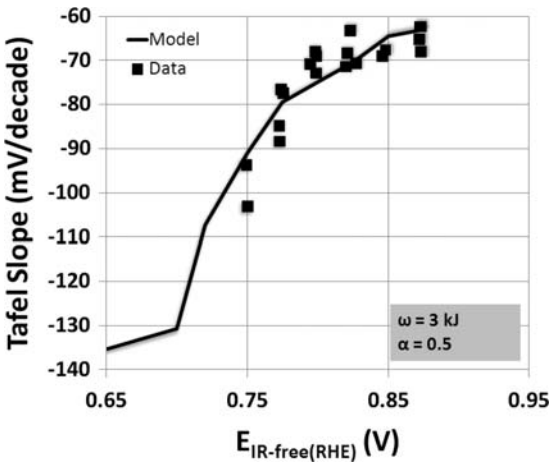

Figure 8. Fit of coverage-dependent Tafel-slope model to the apparent experimental Tafel-slope at different $E_{IR\text{-}free(RHE)}$.

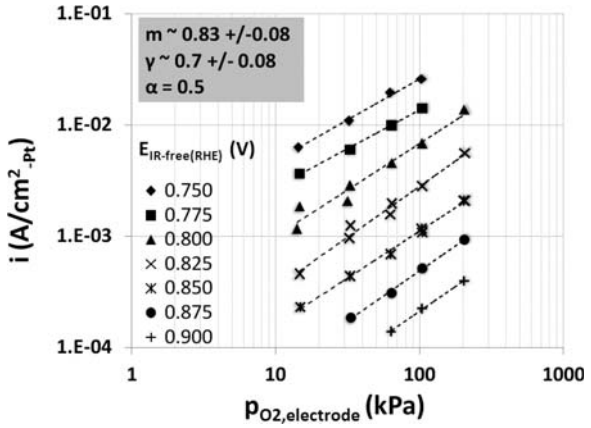

Figure 9. Plot of experimental log(i) vs. log ($p_{O2,electrode}$) at different $E_{IR\text{-}free(RHE)}$ with an average slope of m ($\gamma+\alpha/4$)~0.83 (i.e, $\gamma = 0.7$ for $\alpha = 0.5$).

Tafel-slopes, we assumed the transfer coefficient, $\alpha = 0.5$. Hence the pure kinetic reaction order is ~0.7 (0.83–0.5/4) with a standard deviation of 0.08. Next we used the fitted parameters from Figures 8 and 9 and predicted the apparent kinetic reaction order as a function of $E_{IR\text{-}free(RHE)}$ using the definition given in Table I and this is shown in Figure 10. It is clear that the apparent kinetic reaction order, increases from ~0.55 to ~0.7 as potential decreases from ~0.875 to ~0.65 V vs. RHE. The trends are similar to Uchimura et al.[21] where they report an apparent reaction order of 0.5 to 0.75 from high to low potential (or high to low oxide coverage).

Finally using $\gamma = 0.7$, $\alpha = 0.5$, $\omega = 3.0$ kJ, we fit the experimental polarization curves to the ORR kinetic model to determine i_0. A more convenient representation of the data in Figures 4a and 4b is to convert the x-axis into A/cm$^2_{-Pt}$ using the roughness factor (r.f.) of the electrode as defined in Equations 10 and 11. This results in master plot as shown in Figure 11.

$$\frac{A}{cm^2_{-Pt}} = \frac{\frac{A}{cm^2_{-geo}}}{r \cdot f.} \qquad [10]$$

where,

$$r.f.\left(\frac{cm^2_{-Pt}}{cm^2_{-geo}}\right) = 10 \times Pt\ loading\left(\frac{mg_{-Pt}}{cm^2_{-geo}}\right) \times Pt\ surface\ area\left(\frac{m^2_{-Pt}}{g_{-Pt}}\right) \qquad [11]$$

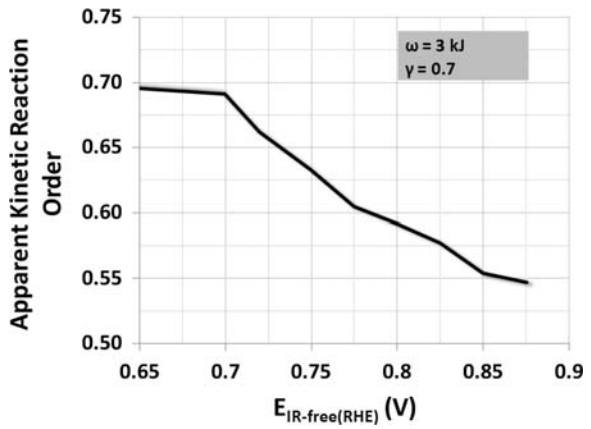

Figure 10. Coverage-dependent apparent kinetic reaction order vs. $E_{IR\text{-}free(RHE)}$ determined by using fit parameters from Figure 8 and Figure 9 in equation in Table I.

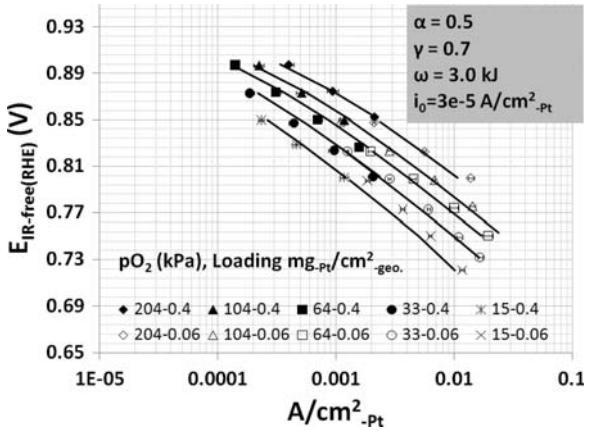

Figure 11. O_2 polarization data normalized to Pt-surface area at varying $p_{O2,channel}$ = 204/104/64/33/15 kPa. The solid and open symbols represent experimental data with ~0.4 mg$_{-Pt}$/cm$^2_{-geo}$ and ~0.06 mg$_{-Pt}$/cm$^2_{-geo}$ loaded cathodes, respectively and the solid lines represent the coverage-dependent kinetic model predictions.

Precise control of gravimetric Pt-loading during electrode fabrication for the different samples within a loading type (especially for the 0.06 mg-Pt/cm$^2_{-geo}$ type) is difficult. These will show up as differences in the observed geometric current density and may contribute to wider error bars seen in Figure 4b. The normalization of the data with r.f. of Pt corrects for such loading differences and almost eliminates the error bars in current density as clearly shown in Figure 11. The fit of the model to the data is also shown in Figure 11. The coverage-dependent model provides a good fit of the experimental data and can predict the transition in Tafel-slope. An i_0 of 3.0×10^{-5} A/cm$^2_{-Pt}$ was used for these fits and the $\mathbf{i_0}^{(0.9\,V)}$ was calculated to be 1.6×10^{-4} A/cm$^2_{-Pt}$. A higher i_0 is predicted by the coverage-dependent kinetics compared to the constant Tafel-slope kinetics. The difference comes from extrapolating a 2.303 RT/F line in Tafel-kinetics vs. extrapolating 2.303*2 RT/F line in the coverage-dependent kinetics. The parameters for the coverage-dependent model are summarized in Table II.

A transfer coefficient, $\alpha = 0.5$ used here in the coverage-dependent kinetics is typical, while $\alpha = 1$ typically used in the simple Tafel-kinetics is unusual. $\omega = 3.0$ kJ is a fitting parameter and is nearly 1/5th as reported previously.[19] Interpretation of the origin for the differences in ω is feasible only with an understanding of ORR mechanism. The coverage-dependent ORR kinetic expression used in this work to explain Tafel-slope transition is still empirical. The Tafel-slope transition may also convey a transition or limitation in ORR mechanism.[14,15] From this work, it is not possible to pinpoint the reaction mechanism based on the estimated kinetic reaction order of 0.7 due to significant standard deviation of 0.08.

The coverage-dependent kinetics could be used instead of constant Tafel-slope kinetics in a fuel cell model to predict performance under real fuel cell operating conditions for low-loaded cathodes, in particular, which is out of scope of this paper. However, it will be interesting, to predict purely kinetic performance for coverage-dependent vs. simple Tafel kinetics at conditions (T, p_{O2}) that could exist in an operating fuel cell. For a fuel cell operating in H_2-Air at ambient P, 80°C, fully saturated conditions, $p_{O2,channel}$ is about 11 kPa. For an ideal cathode it is assumed that 1) there are no electrode proton transport limitations and 2) $p_{O2,electrode}$ is the same as $p_{O2,channel}$. Figure 12 shows kinetic model simulations for $p_{O2,electrode}$ of 11 kPa at 80°C using the parameters for Tafel kinetics vs. coverage-dependent kinetics for two cathode loadings 0.4 and 0.06 mg$_{-Pt}$/cm$^2_{-geo}$ Irrespective of cathode loading, both kinetics show similar performance and apparent Tafel slope above ~ 0.8 V. Below ~0.8 V, the coverage-dependent kinetics shows higher Tafel-slopes and higher losses in cell potential. For the coverage-dependent kinetics, at any given geometric current density, the cathode with 0.06 mg$_{-Pt}$/cm$^2_{-geo}$ loading is at lower po-

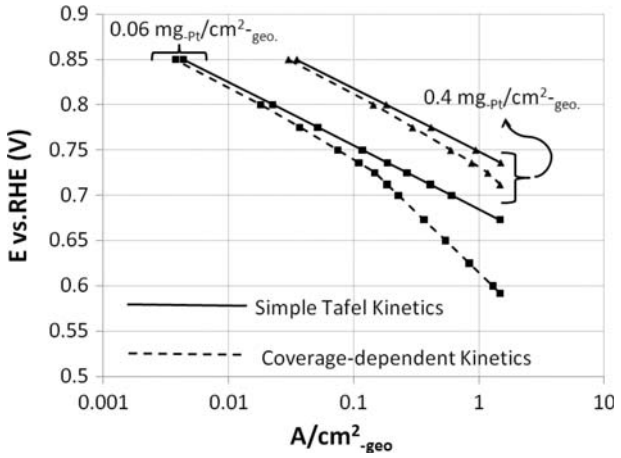

Figure 12. Kinetic model simulations for simple Tafel vs. coverage-dependent kinetics at 11 kPa $p_{O2,electrode}$ and 80°C. The y-axis refers to cell potential vs. RHE determined purely from kinetics.

tential and hence exhibits higher apparent Tafel-slopes compared to 0.4 mg_{-Pt}/cm^2_{-geo} loaded cathode. At the highest current density, 1.5 A/cm^2_{-geo}, ~ 81 and 24 mV additional losses are seen, respectively, for the low (0.06) and high (0.4) loaded cathodes under coverage-dependent kinetics compared to Tafel-kinetics. The dependence of Tafel-slope on potential determined from this work can be used to explain some of the un-explained losses seen with low-loaded cathodes at high current densities that operate at progressively lower potentials compared to 0.4 mg_{-Pt}/cm^2_{-geo} loaded cathodes.

The coverage-dependent model will predict lower Tafel-slopes, lower than 2.303 RT/F at higher potentials (>0.9 V) and higher oxide coverage. Below 0.6 V and zero oxide coverage, the Tafel-slope will be constant at 2.303*2 RT/F. The potential range explored in this work to measure kinetics is still not sufficient to fully test the validity of the coverage-dependent ORR kinetics. There is a limit to the higher potentials that can be reached due to the measurement sensitivity at lower current densities achieved with the loadings and partial pressures used in current work. But, higher potentials can be explored with higher O_2 partial pressure, which is being pursued currently. There is a limit to the lower potentials (and progressively higher current densities) that can be explored due to uncertainty introduced in the kinetic measurements from transport limitations. Correlating ORR transients to oxide kinetics will provide supporting evidence to such coverage-dependent kinetics and is one of the focuses of our ongoing work. Further validation of coverage-dependent kinetics is also necessary at a variety of operating conditions and on different catalysts or electrode structures before we attempt to understand reaction mechanism.

Conclusions

Low-loaded cathode and very low oxygen partial pressures (i.e., pure O_2 in vacuum at full water saturation) were utilized to allow measurement of ORR currents without transport (proton, oxygen, and hydrogen) related losses over a wide range of potentials (0.72 to 0.9 Volts vs. RHE). Above ~0.8 V vs. RHE, the apparent Tafel-slope is nearly constant 2.303 RT/F (70mV/dec. at 80°C). Below 0.8 V vs. RHE the apparent Tafel-slope increases and it increases to ~104 mV/dec. at 750 mV $E_{IR-free(RHE)}$ (at 80°C) and is expected to reach 2.303*2 RT/F (140 mV/dec. at 80°C) by 0.6 V vs. RHE and zero oxide coverage. The coverage-dependent model was used to fit the experimental ORR data and the related intrinsic kinetic parameters have been extracted. The coverage-dependent model could explain some of the additional losses seen with low-loaded cathodes.

Acknowledgments

This work was supported in part by the U.S. Department of Energy under contract # DE-EE0000470. The authors would also like to acknowledge Gregory Sterman, Robert Moses and Travis Downs for fuel-cell testing support.

List of Symbols

Term	Description
E_{Cell}, V	Cell Potential
$E_{IR-free}$, V	iR-free potential
$E_{IR-free(RHE)}$, V	iR-free potential vs. RHE
E_0, V	Reversible potential defined at $p_{O2,ref} = p_{H2,ref} = 101$ kPa
E_{rev}, V	Reversible potential
F, A s/mol	Faraday constant
HFR, Ohm-cm^2	High Frequency Resistance
I, A/cm^2_{-geo}	Geometric current density
i, A/cm^2_{-Pt}	Current density (normalized to available Pt-surface area)
i_0, A/cm^2_{-Pt}	Exchange current density
$i_0^{(0.9\,V)}$, A/cm^2_{-Pt}	Exchange current density calculated at 0.9 V vs. RHE
m	Kinetic + Thermodynamic or Total reaction order
p_{O2}, kPa	Oxygen partial pressure
$p_{O2,channel}$, kPa	Oxygen partial pressure in the channel
$p_{O2,electrode}$, kPa	Oxygen partial pressure in the electrode
p_{H2}, kPa	Hydrogen partial pressure
$p_{O2,ref}$, kPa	Reference oxygen partial pressure
$p_{H2,ref}$, kPa	Reference hydrogen partial pressure
RHE	Reversible Hydrogen Electrode
$R_{H^+}^{cathode}$, Ohm-cm^2	Proton transfer resistance in the cathode
R, J/mol/K	Gas Constant
T, K	Temperature
α	Electron transfer coefficient
γ	Kinetic oxygen reaction order
ω, J	Energy parameter for oxide adsorption
η, V	Overpotential for ORR
θ	Oxide coverage
Q_o, A s	Oxide charge
Q_H, A s	Hydrogen adsorption charge

References

1. K. C. Neyerlin, W. Gu, J. Jorne, and H. A. Gasteiger, *J. Electrochem. Soc.*, **154**, B631 (2007).
2. K. C. Neyerlin, W. Gu, J. Jorne, and H. A. Gasteiger, *J. Electrochem. Soc.*, **153**, A1955 (2006).
3. T. J. Schmidt, U. A. Paulus, H. A. Gasteiger, and R. J. Behm, *J. Electroanal. Chem.*, **508**, 41 (2001).
4. O. Antoine, Y. Bultel, and R. Durand, *J. Electroanal. Chem.*, **499**, 85 (2001).
5. E. Guilminot, A. Corcella, M. Chatenet, and F. Maillard, *J. Electroanal. Chem.*, **599**, 111 (2007).
6. S. Chen and A. Kucernak, *J. Phys. Chem. B*, **108**, 3262 (2004).
7. A. Parthasarathy and C. R. Martin, *J. Electrochem. Soc.*, **138**, 916 (1991).
8. R. Subbaraman, D. Strmcnik, V. Stamenkovic, and N. Markovic, *J. Phys. Chem. C*, **114**, 8414 (2010).
9. J. K. Nørskov, J. Rossmeisl, A. Logadottir, L. Lindqvist, J. R. Kitchin, T. Bligaard and H. Jo´nsson, *J. Phys. Chem. B.*, **108**, 17886 (2004).
10. R. Makharia, N. Subramanian, S. Kumaraguru, T. Greszler, B. Litteer, and Z. Liu, *Fuel Cell Seminar and Exposition*, Phoenix, AZ, Presentation # GHT 33-2 (2008).
11. Y. Ono, T. Mashio, S. Takaichi, A. Ohma, H. Kanesaka, and K. Shinohara, *ECS Transactions*, **28**(27), 69 (2010).
12. S. Gottesfeld, *ECS Transactions*, **6**(25), 51 (2008).
13. F. A. Uribe, M. S. Wilson, and S. Gottesfeld, *Electrochem. Soc. Proc.*, **92**(11), 494 (1992).
14. J. X. Wang, F. A. Uribe, T. E. Springer, J. Zhang, and R. R. Adzic, *Faraday Discussions*, **140**, 347 (2008).
15. J. X. Wang, J. Zhang, and R. R. Adzic, *J. Phys. Chem. A.*, **111**, 12702 (2007).
16. H. Angerstein-Kozlowska, B. E. Conway, and W. B. A. Sharp, *J. Electroanal. Chem.*, **43**, 9 (1973).

17. D. B. Sepa, M. V. Vojnovic, Lj. M. Vracar, and A. Damjanovic, *Electrochim. Acta*, **31**, 91 (1986).
18. Y. Suzuki, S. Sugawara, N. Horibe, S. Kocha, and K. Shinohara, *214th* ECS Meeting, Honolulu, HI, Abstract No. 919, Fall (2008)
19. N. M. Markovic´, H. A. Gasteiger, B. N. Grgur, and P. N. Ross, *J. Electroanal. Chem.*, **467**, 157 (1999).
20. A. Weber and J. Newman, *Chem. Rev.*, **104**, 4679 (2004).
21. M. Uchimura and S. Kocha, 214th ECS Meeting, Abstract No. 914, Fall (2008)
22. H. A. Gasteiger, S. S. Kocha, B. Sompalli, and F. T. Wagner, *Applied Catalysis B: Environmental*, **56**, 9 (2005).
23. R. N. Carter, S. S. Kocha, F. Wagner, M. Fay, and H. A. Gasteiger, *ECS Trans.*, **11**(1), 403 (2007).
24. Y. Liu, M. W. Murphy, D. R. Baker, W. Gu, C. Ji, J. Jorne, and H. A. Gasteiger, *ECS Trans.*, **11**(1), 473 (2007).
25. K. C. Neyerlin, W. Gu, J. Jorne, A. Clark, Jr. , and H. A. Gasteiger, *J. Electrochem. Soc.*, **154**, B631 (2007).
26. M. F. Mathias, D. R. Baker, J. Zhang, Y. Liu, and W. Gu, *ECS Trans.*,**13**(13), 129 (2008).
27. Y. Liu, M. Mathias, and J. Zhang, *Electrochem. Solid State Lett.* **13**, B1 (2010).
28. K. Kudo, T. Suzuki, and Y. Morimoto, *ECS Trans.*, **33**(1), 1495 (2010).
29. N. Nonoyama, S. Okazaki, A. Z. Weber, Y. Ikogi, and T. Yoshida, *J. Electrochem. Soc.*, **158**, B416 (2011).
30. M. Teliska, W. E. O'Grady, and D. E. Ramaker, *J. Phys. Chem. B*, **109**, 8076 (2005).
31. M. Wakisaka, H. Suzuki, S. Mitsui, H. Uchida, and M. Watanabe, *J. Phys. Chem. C*, **112**, 2750 (2008).
32. C. H. Paik, T. D. Jarvi, and W. E. O'Grady, *Electrochem. Solid-State Lett.*, **7**, A82 (2004).